NANO · MICRO small
www.small-journal.com

Multifunctional Antimicrobial Biometallohydrogels Based on Amino Acid Coordinated Self-Assembly

Jingwen Song, Chengqian Yuan, Tifeng Jiao, Ruirui Xing, Mengyao Yang, Dave J. Adams,* and Xuehai Yan**

There is a real need for new antibiotics against self-evolving bacteria. One option is to use biofriendly broad-spectrum and mechanically tunable antimicrobial hydrogels that can combat multidrug-resistant microbes. Whilst appealing, there are currently limited options. Herein, broad-spectrum antimicrobial biometallohydrogels based on the self-assembly and local mineralization of Ag^+-coordinated Fmoc-amino acids are reported. Such biometallohydrogels have the advantages of localized delivery and sustained release, reduced drug dosage and toxicity yet improved bioavailability, prolonged drug effect, and tunable mechanical strength. Furthermore, they can directly interact with the cell walls and membrane, resulting in the detachment of the plasma membrane and leakage of the cytoplasm. This leads to cell death, triggering a significant antibacterial effect against both Gram-negative (*Escherichia coli*) and Gram-positive (*Staphylococcus aureus*) bacteria in cells and mice. This study paves the way for developing a multifunctional integration platform based on simple biomolecules coordinated self-assembly toward a broad range of biomedical applications.

1. Introduction

Bacterial infections are one of the world's major public health challenges and the wide spread of multidrug-resistance to currently available antibiotics poses a serious concern to global healthcare.[1] There has been significant effort devoted to develop new alternative antimicrobial materials, such as cationic polymers,[2] antibacterial peptides,[3] and metal nanoparticles[4] for the treatment of bacterial infections. However, cationic polymers suffer from long-term biosafety due to their nondegradable backbones and long-term toxicity, hampering their further clinical applications.[5] Although antibacterial peptides are emerging as potential candidates for overcoming the drawbacks of cationic polymers, the majority of these are subject to limitations associated with hemolysis and cytotoxicity, short half-life in vivo as well as high manufacturing cost.[6] As a broad-spectrum antimicrobial agent, metal nanoparticles, especially silver nanoparticles (AgNPs), are known to exhibit strong antibacterial activities yet low microbial resistance compared to antibiotics and small molecular biocides.[4a] Indeed, AgNPs-containing antibacterial dressings have showed clinical success to some extent.[7] Nevertheless, individual AgNPs are still not perfect solutions as replacements for antibiotic drugs because AgNPs may accumulate in the tissues. Ag^+ may also cause local or systemic side effects at high dosages or prolonged use, such as allergic reactions, skin staining, and cellular toxicity.[8] Hence, there is a real need to develop potent and broad-spectrum antibacterial agents with low propensity for drug-resistance development whilst maintaining high biocompatibility and biosafety.

Dr. J. Song, Prof. T. Jiao
State Key Laboratory of Metastable Materials Science and Technology
Yanshan University
Qinhuangdao 066004, P. R. China
E-mail: tfjiao@ysu.edu.cn

Dr. J. Song, Dr. C. Yuan, Dr. R. Xing, Dr. M. Yang, Prof. X. Yan
State Key Laboratory of Biochemical Engineering
Institute of Process Engineering
Chinese Academy of Sciences
Beijing 100190, P. R. China
E-mail: yanxh@ipe.ac.cn

The ORCID identification number(s) for the author(s) of this article can be found under https://doi.org/10.1002/smll.201907309.

DOI: 10.1002/smll.201907309

Dr. M. Yang, Prof. X. Yan
School of Chemical Engineering
University of Chinese Academy of Sciences
Beijing 100049, P. R. China

Prof. D. J. Adams
School of Chemistry
University of Glasgow
Glasgow G12 8QQ, UK
E-mail: dave.adams@glasgow.ac.uk

Prof. X. Yan
Center for Mesoscience
Institute of Process Engineering
Chinese Academy of Sciences
Beijing 100190, P. R. China

As an alternative strategy, antimicrobial hydrogels with an intrinsic antimicrobial activity or loaded with antibacterial drugs are becoming a promising platform for the controlled release of antimicrobial agents to tissue locally.[9] Because of their excellent biocompatibility and natural abundance, an extensive range of biomolecules such as collagen, peptides, and amino acids have been used as the building blocks for preparation of antimicrobial hydrogels.[2b,10] Out of these, amphiphilic amino acids such as leucine and proline modified with aromatic groups have attracted attention due to their ready availability, cost effectiveness, inherent anti-inflammatory, and antibacterial properties.[11] Although they may have potential for developing the antimicrobial agents, these amino acid hydrogels have a poor rheology and suffer from rapid transformation into thermodynamically favorable crystalline precipitates (especially when subject to external shearing).[12] In addition, amino acid-based hydrogels usually have narrow-spectrum antibacterial activities due to their specific molecular recognition, disabling their effective therapy and development of related formulation for bacterial infections.[13] Therefore, there remains a significant challenge to design and develop biocompatible, broad-spectrum, and mechanically tunable antibacterial hydrogels based on simple biomolecule combinations.

Herein, we propose a biometallohydrogel with broad-spectrum antimicrobial activities and tunable mechanical properties based on biocompatible amino acid coordinated self-assembly with Ag^+. The high directionality and anchoring ability of the coordination interactions allow Ag^+ to be fixed within the amino acid nanofiber hydrogels, where the Ag^+-Fmoc-amino acid coordination complexes act as precursors for producing AgNPs through a mild mineralization process (**Scheme 1**). In situ mineralization of AgNPs ensures the controlled spatial distribution of AgNPs in the hydrogel matrix, which is of key importance for sustainable release of Ag^+, improved antimicrobial efficacy and tunable mechanical properties.[14,15a] It has been reported that several *N*-(fluorenyl-9-methoxycarbonyl) (Fmoc)-modified amino acids possess inherent antimicrobial activities and good biocompatibility.[9a,11b,14] By screening Fmoc-amino acids (Figure S1, Supporting Information), we found four can form metallohydrogels based on the coordination interaction between Fmoc-amino acids and Ag^+ in addition to the multiple noncovalent interactions between Fmoc-amino acids. The resulting biometallohydrogels exhibit advantages as in vivo antimicrobial materials compared to the traditional AgNPs-containing peptide assemblies.[16] First, the present strategy is facile and flexible for the design of antibacterial metallohydrogels with good biocompatibility and biodegradability. Second, the interaction between AgNPs and amino acids not only effectively prevents the self-aggregation and improves the stability of AgNPs, but also imparts the biometallohydrogels tunable mechanical properties. Third, the controlled and locally sustained release of antimicrobial amino acids and AgNPs from the metallohydrogel can effectively lower the drug dosage and toxicity, prevent biofilm formation, improve bioavailability, and prolong drug effect. Moreover, metallohydrogels exhibit potent antimicrobial activity against both Gram-negative (*Escherichia coli*) and Gram-positive (*Staphylococcus aureus*) bacteria and boost the in vivo therapeutic effects on an infected rat model.

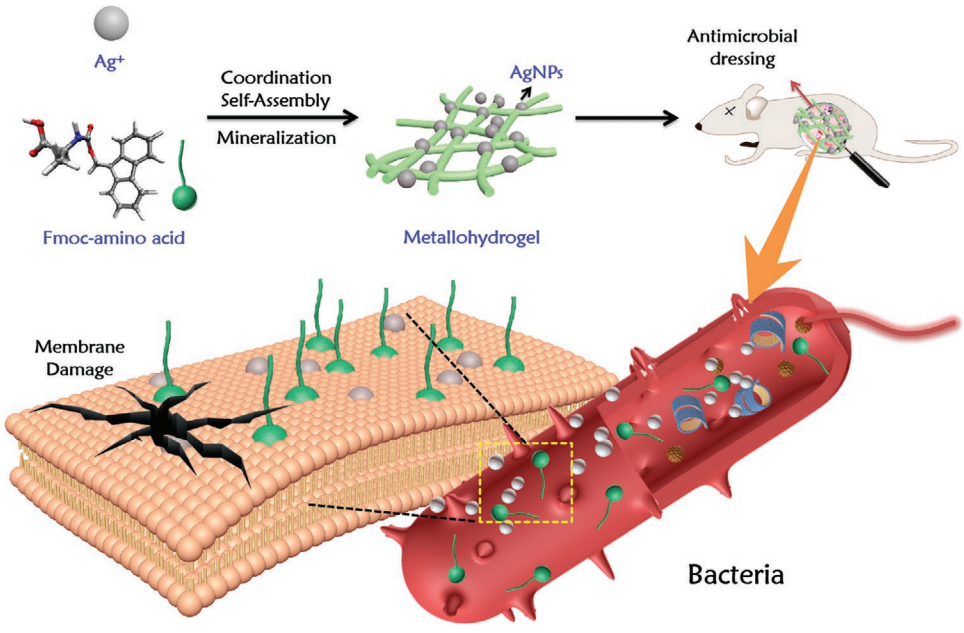

Scheme 1. Schematic diagram of the formation of Ag^+-coordinated Fmoc-amino acid metallohydrogels based on coordinated self-assembly and local mineralization, and their application as antimicrobial dressing. AgNPs of small size and high dispersion are formed in the biometallohydrogels. Such biocompatible metallohydrogels exhibit enhanced antibacterial activity due to the synergy between amphiphilic amino acids and broad-spectrum antibacterial AgNPs. Amphiphilic amino acids released from the metallohydrogels permeate the cell walls and membrane through hydrophobic interactions, followed by substantial disruption to bacterial morphology. Both Ag^+ and AgNPs are able to directly interact with bacterial cells, which can cause morphological changes of cell wall and permeability changes of cell membrane. This would result in the detachment of the plasma membrane and the leakage of the cytoplasm, hence leading to cell death.

2. Results and Discussion

Our Fmoc-amino acid metallohydrogels are fabricated through amino acid coordinated self-assembly with Ag^+. Typically, Fmoc-amino acids are dissolved in Tris (hydroxymethyl) aminomethane–HNO_3 and rapidly mixed with Ag^+ solution under ambient conditions. The centrifuge tubes were wrapped in aluminum foil to prevent the irradiation of light. The solutions became turbid immediately and formed hydrogels after different incubation times (3, 10, 16 h and 5 day for Fmoc-P, Fmoc-H, Fmoc-A, and Fmoc-L, respectively). For these four Fmoc-amino acids, gels form only with the presence of coordination interaction between amino acids and Ag^+ (as shown by the photographs in **Figure 1** and Figure S1 (Supporting Information)). The introduction of Ag^+ coordination enhances the nonspecific hydrophobic interactions between the Fmoc-amino acids, which trap the hydrogel in a metastable state.[17] The robust hydrophobic interactions hinder the further molecular rearrangement and long-range ordered molecular packing through hydrogen bonding and π–π stacking, hence inhibiting the formation of crystalline aggregates. For other Fmoc-amino acids, no gels formed under these conditions (Figure S1, Supporting Information). Transmission electron microscopy (TEM) and atomic force microscopy (AFM) images of the samples indicate the formation of intertwined nanofibers (Figure 1; Figure S2, Supporting Information), which are ≈20 nm in diameter and several micrometers in length. AgNPs not exceeding 6 nm in size were found uniformly dispersed within the Fmoc-amino acids nanofibers. The AgNPs are spatially ordered along the long axes of hydrogel fibers, which effectively prevent the self-aggregation and improve the stability of AgNPs.

This is further verified by the UV–vis absorption spectroscopy (Figure S3a, Supporting Information), where no characteristic surface plasmon resonance absorption of AgNPs around 400 nm is observed.[15a] XPS shows signals at 368.5 and 374.5 eV with the interval of 6.0 eV, respectively, which corresponds to the binding energies of Ag $3d_{5/2}$ and Ag $3d_{3/2}$, confirming the formation of AgNPs from the Ag^+-coordinated Fmoc-amino acids complexes (Figure S3b, Supporting Information).[15b] The high-resolution TEM (HR-TEM) images (insets in Figure 1) demonstrate the presence of a lattice plane with an interfringe distance of 2.35 Å, which corresponds to the (111) plane of Ag.[18] All these results demonstrate that well-dispersed AgNPs are formed in situ in the hydrogel network.

When the samples were prepared without protection of aluminum foil, irradiation by sunlight resulted in the formation of hydrogels with a light yellow or pink color (Figure S4, Supporting Information). The AgNPs formed in these systems were larger and dispersed both on the nanofibers and in the

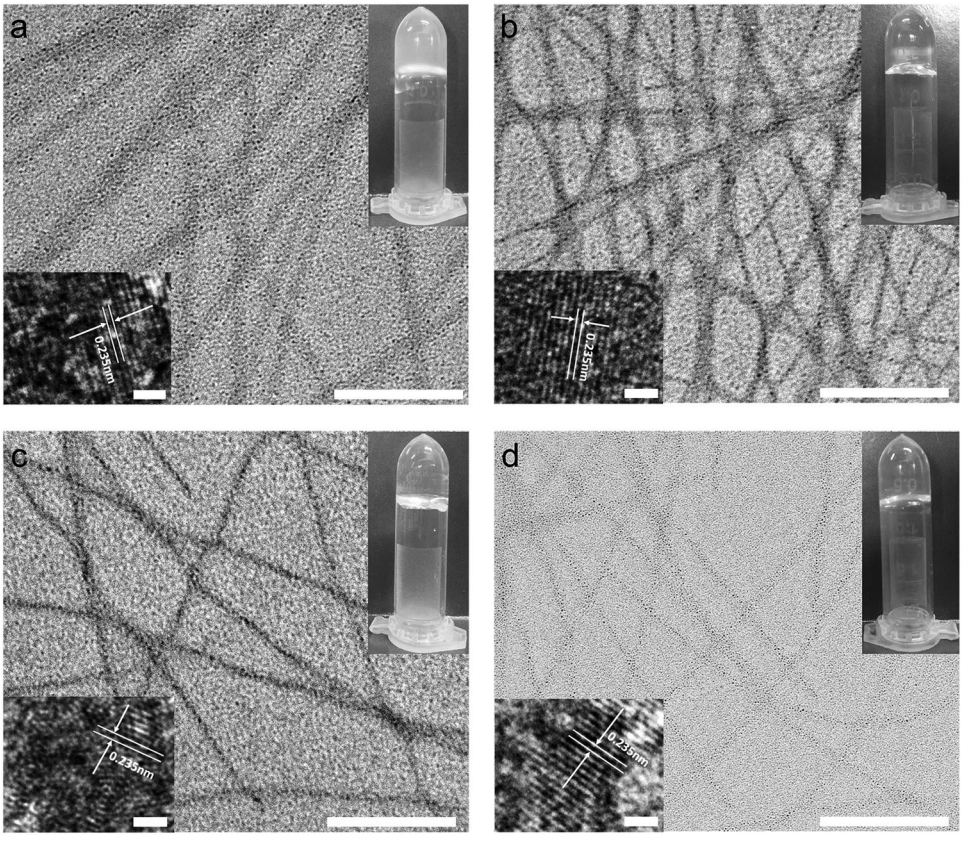

Figure 1. TEM images of the biometallohydrogels based on Ag^+-coordinated Fmoc-amino acids self-assembly. a) Fmoc-His, b) Fmoc-Pro, c) Fmoc-Ala, and d) Fmoc-Leu. The photographs of inverted tubes inserted confirm the formation of hydrogel. The HR-TEM images inserted clearly show the (111) plane of AgNPs locally dispersed within the metallohydrogel nanofibers. All the scale bars in the TEM images are 200 nm and inserted HR-TEM images are 1 nm. The samples were freshly prepared (with 4 mg mL^{-1} Fmoc-amino acids and 8×10^{-3} M Ag^+) and aged for 5 days before characterization.

bulk solution (Figure S4, Supporting Information). The formation of ultrasmall AgNPs in the original samples is attributed to the hydroxyl group of the Tris-HNO_3 buffer, which serves as an in situ reductant to form the AgNPs. Such a mineralization process, without introduction of photoirradiation or a reductant such as sodium borohydride, minimizes the undesired toxicity and maximizes the biocompatibility. In addition, Fmoc-amino acids are also able to bind AgNPs either through the C=O from the Fmoc or carboxyl groups, which prevent their agglomeration and ensure the stability of AgNPs.[19]

We then investigated the molecular mechanism underlying the formation of the amino acid metallohydrogels. The characteristic peaks of amino acid–Ag^+ coordination complexes were found in the electrospray ionization mass spectra of metallohydrogels (Figure S5, Supporting Information), which clearly confirmed the presence of coordination interaction between Fmoc-amino acids and Ag^+. Obvious shifts of stretching vibration of carboxyl in Fourier transform infrared (FTIR) spectra revealed the presence of coordination interaction between the carboxylate groups and Ag^+ (Figure S6, Supporting Information).[20] Furthermore, optimized coordination modes between Fmoc-amino acids and Ag^+ were obtained from density functional theory calculations (Figure S6, Supporting Information). The molecular lengths of amino acid coordinated complexes are close to the *d*-spacings calculated from the X-ray diffraction (XRD) spectra (Figure S7, Supporting Information). Moreover, the FTIR spectra demonstrate the intermolecular hydrogen bonds between neighboring carbamate groups (N—H···O) in the metallohydrogels, which exhibit similar β-sheet structure to proteins and polypeptides (Figures S6 and S8, Supporting Information).[21] In addition, red-shifts of the characteristic emission signal of fluorenyl group in metallohydrogels compared to those of the Fmoc-amino acid monomer solutions and the presence of excimer peaks shows that the π–π stacking interactions also contributed to the stabilization of hydrogels (Figure S9, Supporting Information).[22] Therefore, coordination interaction and intermolecular hydrogen bonding interactions (C=O···H—N and C=O···H—O) as well as π–π stacking drive the formation of Fmoc-amino acids metallohydrogels.

Concentration-dependent rheological properties of the Fmoc-Ala metallohydrogels formed with different starting concentration of Ag^+ were measured (**Figure 2**a). The storage and loss oscillatory shear moduli (G' and G'', respectively) confirm the hydrogel-like behavior at the starting concentration of Ag^+ ranging from 4 to 10×10^{-3} M. G' and G'' simultaneously increase until the Ag^+ concentration reached at 8×10^{-3} M, indicating the modulation role of coordination interactions on the mechanical properties of amino acid hydrogels. However, excessive coordination-enhanced hydrophobic interactions are unfavorable for the formation of metallohydrogels, as evidenced by the macroscopic precipitation formed with Ag^+ concentration of 15×10^{-3} M (Figure S10, Supporting Information). The angular frequency-dependent rheological properties of the metallohydrogels with a Ag^+ concentration of 8×10^{-3} M show the

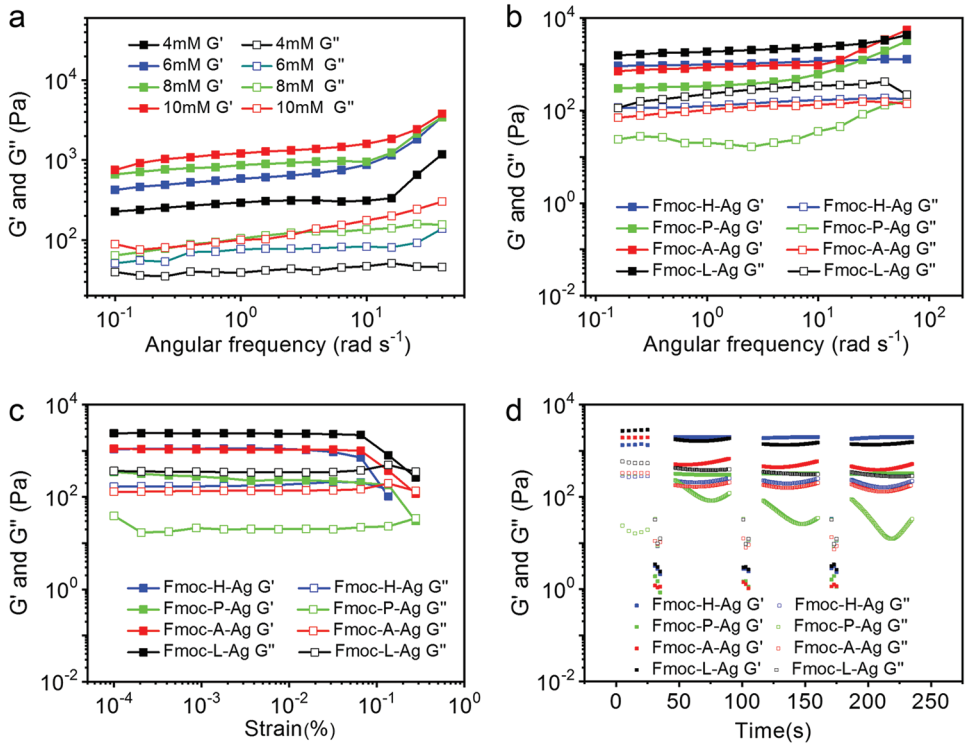

Figure 2. Rheological properties of Fmoc-amino acid metallohydrogels. a) Frequency-dependent storage (G') and loss (G'') moduli of the Fmoc-Ala metallohydrogels with different Ag^+ concentration. b) Frequency-dependent rheological properties of the metallohydrogels. c) Strain-dependent oscillatory rheological properties of the metallohydrogels. d) Self-healing property of the metallohydrogels demonstrated by the continuous step-strain measurements, which were carried out in steps of 500% and 1% oscillatory strain for three cycles. The solid and hollow squares represent storage (G') and loss (G'') moduli, respectively. The metallohydrogels used in (b–d) were prepared with an amino acid concentration of 4 mg mL^{-1} and Ag^+ concentration of 8×10^{-3} M. All the hydrogels were aged for 5 days before characterization.

dominant role of the storage modules and the tangent values of the phase angle (G''/G') less than unity across the range of frequencies observed (Figure 2b; Figure S11, Supporting Information).[23] Strain-dependent oscillatory rheology (Figure 2c) of the Fmoc-amino acid metallohydrogels exhibits shear-thinning behavior.[10a] Continuous step change of the oscillatory strain between 500% and 1% at the same frequency (1 rad s^{-1}) can be used to assess the strain-induced damage and self-healing property of the Fmoc-amino acid metallohydrogels (Figure 2d). The results reveal that the structures recover quickly and display a normal hydrogel-like behavior over three cycles of breaking and reforming. The strength of Fmoc-amino acids (except Fmoc-Ala) metallohydrogels was more than 60% recovered as compared to the original hydrogels, which are most likely due to the hydrogen bonding interactions between Fmoc-amino acids. Adjustment in rheological properties by altering the concentration of Ag^+, and so the content of Ag NPs, allows us to prepare injectable metallohydrogels. Metallohydrogels with an Ag^+ concentration of 8×10^{-3} M exhibited shear-thinning and self-healing features, making them suitable for biomedical applications such as antimicrobial dressings with convenient coating and painless removal, dramatically reducing the chance of secondary trauma.[24]

We then used the amino acid metallohydrogels as antimicrobial materials for bacterial infections therapy. We first examined the antibacterial activity of these biometallohydrogels using Oxford cup methods through comparison with the same concentration of Ag^+ solution, Fmoc-amino acid solution and phosphate-buffered saline (PBS) buffer on Luria–Bertani (LB) agar plates. Gram-negative (*E. coli*) and Gram-positive (*S. aureus*) were selected as the model bacteria, as these are most prevalent pathogen to humans. The growth inhibition test of bacteria (**Figure 3**a) demonstrates that Fmoc-amino acid metallohydrogels give rise to larger inhibition zones around

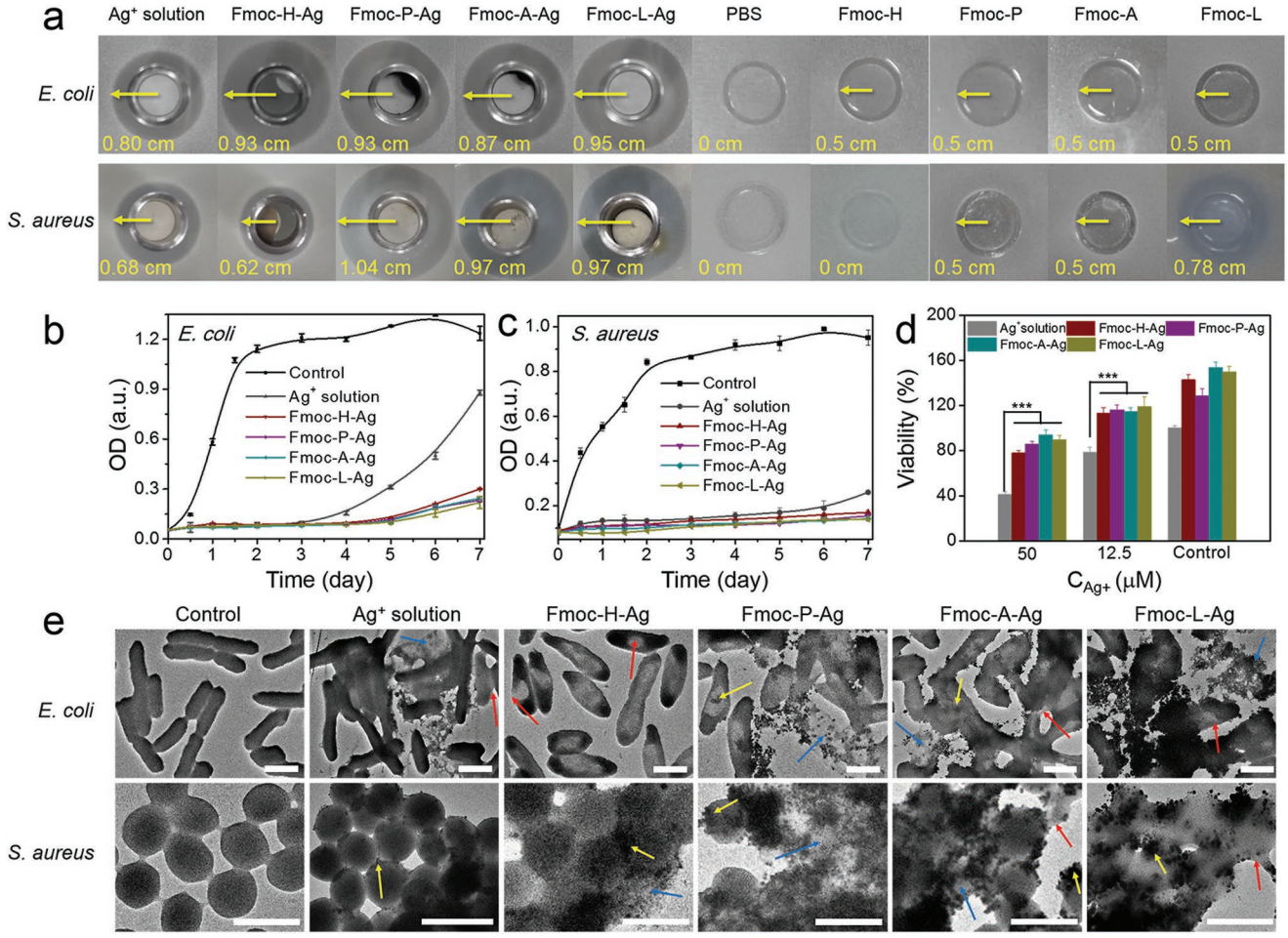

Figure 3. Antibacterial activity and mechanism of Fmoc-amino acid metallohydrogels (prepared with 4 mg mL^{-1} amino acid and 8×10^{-3} M Ag^+). a) Growth inhibition assay created by Fmoc-amino acid metallohydrogels, Ag^+ solution with equivalent amount of Ag^+, Fmoc-amino acids, and PBS solution against *E. coli* and *S. aureus* in the disk diffusion test. The photographs were taken after incubation at 37 °C overnight. b,c) Time-dependent growth inhibitions of bacteria treated with Fmoc-amino acid metallohydrogels, Ag^+ solution, and control group (PBS buffer solution). d) Cell viability (using an MTT assay) of 3T3 with Fmoc-amino acid metallohydrogels and Ag^+ solution with equivalent amount of Ag^+ at the incubation time of 24 h. Results show the mean of the measurements conducted in triplicate ± standard deviation, $^{***}P < 0.001$ (one-way ANOVA). e) Morphological studies of bacteria untreated and treated with Fmoc-amino acid metallohydrogels and Ag^+ solution, where the red, yellow, and blue arrows indicated membrane fusing, clumping, and disintegration. All the scale bars in (e) are 1 μm. The bacterial suspensions (*E. coli* and *S. aureus*) used for tests were within 10^5 to 10^6 CFU mL^{-1}.

the Oxford cups against both *E. coli* and *S. aureus* compared to those treated with individual Fmoc-amino acid solutions. The microbial proliferation was assessed by optical density (OD) measurement, which allows for estimation of the concentration of bacterial cells in a liquid (Figure 3b,c). The OD value of Fmoc-amino acid metallohydrogels treated bacteria did not increase for a period of 7 days in a certain concentration range, significantly suppressing the bacteria growth compared to the Ag^+ solution. This indicates that the antibacterial activity of the Fmoc-amino acid metallohydrogel against both *E. coli* and *S. aureus* is superior to that of Ag^+ solution. Moreover, the metallohydrogels have lower minimum inhibitory concentrations (around 0.4×10^{-3} M Ag and 0.2 mg mL^{-1} Fmoc-amino acids) against both *E. coli* and *S. aureus* compared to the individual Ag^+ and Fmoc-amino acid solution (Figures S12 and S13, Supporting Information). This can be ascribed to the synergistic antimicrobial effect of Fmoc-amino acids and AgNPs against bacterial growth, leading to a relative lower OD value compared to the control experiment after 48 h. Fmoc modification may have a potential role in killing bacteria through its hydrophobic interaction with hydrophobic sections of bacterial cell membrane, as employed by antimicrobial peptides.[25] Compared with individual Ag^+ solution, the Fmoc-amino acid metallohydrogels, especially those with high mechanical strength and stability, could serve as a reservoir for the sustained release of Ag^+ and amphiphilic amino acids, which effectively prolongs the inhibition time of bacteria growth. Moreover, the antimicrobial efficacy of metallohydrogels is further enhanced by the ultrasmall size for high Ag atom efficiency and locally high concentration of Ag^+ assembled on the surface.[26] We used the 3-(4,5-dimethylthiazolyl-2)-2,5-diphenyltetrazolium bromide (MTT) cell survival assay to quantitatively assess the toxicity effect of metallohydrogels on the normal cell. For 3T3 cells, the Ag^+ solution shows a more significant inhibition than the Fmoc-amino acid metallohydrogels in a dosage-dependent manner (Figure 3d). This shows that the Fmoc-amino acids metallohydrogels exhibit fewer toxicological side effects than Ag^+ at the administration dosage range, which is consistent with other work.[27] This result suggests we have highly biocompatible Fmoc-amino acid metallohydrogels.

It also should be noted that some kinds of Fmoc-amino acid metallohydrogels exhibit remarkable antibacterial activities against *S. aureus* (Figure 3a) compared to bare Ag^+. In general, the stiffness and the extensively cross-linked cell wall of Gram-positive bacteria not only reduces the bacterial cell wall anchoring sites for Ag^+ but also renders the Ag^+ more difficult to penetrate.[28] This greatly reduces the ability of Ag^+ to kill Gram-positive bacteria. Previous work found that some kinds of Fmoc-amino acids, such as Fmoc-Leu, can bind to *S. aureus* cell walls rapidly and effectively.[29] We also observed that the Fmoc-Leu/Pro/Ala solution inhibits the growth of Gram-positive bacteria. Hence, we suspect that the sterilization mechanism of the Fmoc-amino acids metallohydrogels is that the Fmoc-amino acids break the rigid structure of the cell walls and cell membrane of the Gram-positive bacteria, and then AgNPs and Ag^+ penetrate into cells more efficiently. The synergy between the two components endows the metallohydrogels with a more potent antimicrobial efficiency against Gram-positive bacteria. Fmoc-His metallohydrogel exhibits a decreased ability to kill Gram-positive bacteria compared to Fmoc-Leu/Pro/Ala metallohydrogels and bare Ag^+ solution. We speculate that this is due to the relatively weak mechanical strength of Fmoc-His metallohydrogel.

To gain insight into the antimicrobial mechanism of the Fmoc-amino acid metallohydrogels, the morphological changes of bacteria after contact with hydrogels and the Ag^+ solution were investigated. As shown in Figure 3e and Figure S14 (Supporting Information) both the untreated *E. coli* and *S. aureus* bacteria cells display typical rod- and sphere-shaped structures with clear edges and smooth bodies. In sharp contrast, cellular deformation and structure collapse are observed in the hydrogel-treated bacteria. Membrane fusing, clumping and disintegration are also abundant in these bacteria, which appeared deflated. Cellular debris as well as lysis of the cells are also evident. The abundant perturbations and severe morphology disruption caused by metallohydrogels imply that the bacteria membrane is the main target of antimicrobial metallohydrogels, which is analogous to action mechanism of cationic antimicrobial peptides. With respect to the bacteria cells exposed to Ag^+ solution (Figure 3e), detachment of the cytoplasm membrane from the cell wall and wrinkled cell walls can be found on *E. coli* cells and numerous nanoparticles accumulate on the surface of the *S. aureus* bacteria cells due to their thick and compact cell membrane. More interestingly, the bacteria cell surfaces also become rough after incubation with individual amino acids solutions at the same concentration with metallohydrogels (Figure S15, Supporting Information). Notably, some of the cells cracked in the Fmoc-Leu treated bacteria. This implies that the Fmoc-amino acids metallohydrogel achieve their antimicrobial effect against bacteria by disrupting the cell walls and membrane and eventually killing the bacteria. Initially, uptake of the metallohydrogel with the assistance of electrostatic attraction between the Ag^+-Fmoc-amino acids coordination complexes and the peptidoglycans of the cell membrane. Then, amphiphilic amino acids and Ag^+ released from the metallohydrogels permeate the cell membrane through the hydrophobic interactions between the Fmoc groups of amino acids and the hydrophobic sections of bacterial cell membrane and the relatively larger volume of the AgNPs, thus destabilizing the membrane and leading to cell death.

Encouraged by the positive antimicrobial activity of Fmoc-amino acids metallohydrogels, we investigated their potential application as an injectable antimicrobial dressing for healing impaired skin wound by a dorsal wound model of mice inoculate to *S. aureus*. We selected the Fmoc-amino acids metallohydrogels and silver sulfadiazine (SSD) cream (traditional wound dressing) as coatings on the wounds, while the control group were left undressed. **Figure 4**a and Figure S16 (Supporting Information) depict the optical microscopic images of small wound cuts (1 cm in length) treated with different dressings in the wound area after infection with *S. aureus* for 4, 8, and 12 days. No obvious inflammation and size difference of wound are observed on the groups treated by Fmoc-amino acid metallohydrogels and SSD, while slight infection emerged from the control group after 4-day treatment (Figure S16, Supporting Information). On extending the treatment time to 8 days (Figure S16, Supporting Information), the wound size began to reduce for the metallohydrogel group. Moreover, the

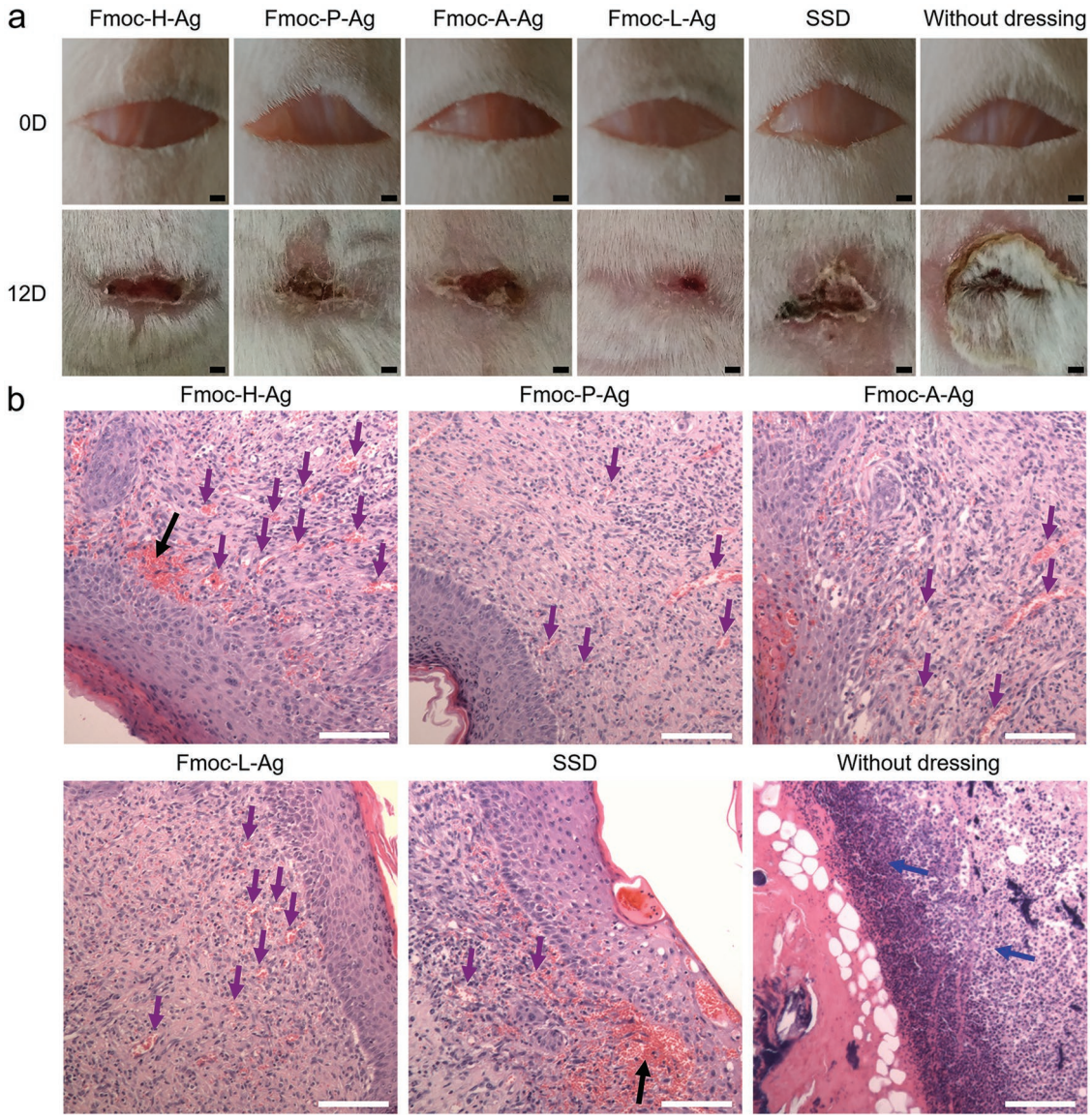

Figure 4. In vivo evaluations of the metallohydrogels for wound healing. a) Visual observation of surface healing upon small wounds with the infection of *S. aureus* for 0 and 12 days (scale bar = 0.1 cm). b) Photomicrographs of skin tissues with H&E staining for treating with hydrogel, SSD, and without dressing after 12 days, where blue, purple, and black arrows indicate inflammatory cells, blood vessel, and local hyperemia, respectively (scale bar = 100 μm). The metallohydrogels were prepared with 8×10^{-3} M Ag^+ and 4 mg mL^{-1} Fmoc-amino acids.

sizes of wounds treated by metallohydrogels and SSD were significantly smaller than those of control groups for *S. aureus*-infected wounds. It is noteworthy to mention that Fmoc-Leu hydrogels reduce the size of the wounds more effectively than other amino acids after treatment for 12 days (Figure 4a).

This result is consistent with the in vitro testing, which showed that the Fmoc-Leu metallohydrogels were more effective at inhibiting *E. coli* and *S. aureus*. Furthermore, the wound healing effects of Fmoc-amino acids metallohydrogels on excisional wound in normal noninfected mice were evaluated (Figure S17, Supporting Information) through comparison with the SSD and control groups. It is obvious that the Fmoc-amino acids metallohydrogels tested under the same conditions have significantly better wound healing effects compared to the SSD and control groups.

Wound healing is a specific biological process concerned with the growth and tissue regeneration, which would undergo several stages including hemostasis, inflammation, migration, proliferation, and maturation phases.[15,30] The antimicrobial mechanism was broadly studied by extensive efforts. The Ag^+ and/or AgNPs may interact with the peptidoglycan cell wall of the bacterial, increase membrane permeability, and further induce cell death, or they will interact with bacterial proteins, avoiding DNA replication. Histomorphological determination on wound regeneration in different phase was conducted by H&E staining. Wound regeneration is evaluated by observing the re-epithelization, fibroblast immigration, connective tissue synthesis, infiltration of inflammatory cells, and collagen production.[31] Histological examination on the surrounding tissue of infected wounds at 4th day reveals

that large zones of inflammatory cell infiltrates are observed in both the treated and untreated groups (Figure S18, blue arrows, Supporting Information), but vasodilation and congestion appeared to be severer in wounds treated with SSD and control group than antimicrobial hydrogel (Figure S18, purple arrows, Supporting Information). The excellent hemostasis from our hydrogel dressing could rapidly stop blood bleeding, which might activate inflammatory phase earlier. At the 12th day, in the hydrogels samples the dermis appeared well organized with fewer inflammatory cells and no large area of local hyperemia (Figure 4, black arrows), while the connective tissue appeared better organized compared to the SSD-treated wound. The staining also indicated a well-formed stratified epithelial layer with clear evidence for stratification. Wounds treated with hydrogels displayed significantly fewer inflammatory cells and a well-organized stratified epithelial layer. Numerous blood vessels in the dermis are found in the hydrogel treated wound (Figure 4b, purple arrows). However, in the control group, histological examination showed that skin cells were necrotic and the wound is still dominated by acute inflammatory response, indicating that *S. aureus* infection has not been inhibited. All the histological results indicate that the Fmoc-amino acids metallohydrogels can accelerate the tissue regeneration in the wound healing.

3. Conclusion

In summary, we have demonstrated a simple yet versatile strategy for formation of effective and broad-spectrum antimicrobial biometallohydrogels based on Ag^+-coordinated Fmoc-amino acids self-assembly and local mineralization. The in situ synthesized AgNPs enhance the amino acid hydrogels mechanically modulated property and broad-spectrum antimicrobial activity. These biometallohydrogels have the advantage of allowing the drug dosage to be reduced, prolonging the drug effect, lowering the toxicity, and improving the bioavailability compared to the previous reported antimicrobial agents (Table S1, Supporting Information). We have also demonstrated that antimicrobial efficiency can be significantly enhanced by synergy between amphiphilic amino acids and broad-spectrum antibacterial AgNPs. Moreover, the broad-spectrum and biocompatible metallohydrogels with modulated mechanical properties provide an alternative insight for development of treatment strategy toward a broad range of practical biomedical applications such as antimicrobial dressings for joints skin wound healing and surgical site infections with convenient coating and painless removing. That strategy for formation of amino acid metallohydrogels is envisaged to be generally applicable for creation of a variety of functional hydrogels, starting from simple biomolecules such as short peptide, amino acid, and nucleic acid that are capable of coordinated self-assembly with metal ions.[32]

4. Experimental Section

Materials: Fmoc-L-serine, Fmoc-L-aspartic acid, Fmoc-L-leucine, Fmoc-L-proline, Fmoc-glycine, and Agar were purchased from J&K Scientific Co. Ltd. Fmoc-Phe-OH was purchased from HEOWNS. Fmoc-His-OH was obtained from BACHEM. Fmoc-Tyr-OH and Fmoc-Ala-OH were supplied by Energy Chemical. Tris (hydroxymethyl) aminomethane was obtained from LANYI REAGENT. Silver sulfadiazine was purchased from Sigma. Silver nitrate ($AgNO_3$) was purchased from Alfa Aesar. Peptone, yeast powder, and Beef Extract Powder were supplied by Solarbio. Dulbecco's modified Eagle's medium (DMEM), Dulbecco's PBS was supplied by M&C Gene Technology Ltd. *E. coli* and *S. aureus* were bought from Institute of Microbiology, Chinese Academy of Sciences. Other materials were purchased from Beijing Chemical Co. Ltd. unless otherwise noted. Water was prepared in a double-stage Milipore Milli-Q Plus purification system. All solutions were freshly prepared for immediate use in each experiment.

Preparation of Metallohydrogels: Fmoc-amino acid powder (4 mg) was dissolved in 20 µL pH = 9.14 Tris-HNO_3 buffer with the help of magnetic stirring. 975 µL $AgNO_3$ solution with different concentrations (2, 4, 6, 8, 10, 15 × 10^{-3} M) adjusted by 5 µL of 0.1 M HNO_3 was added to the above mentioned Fmoc-amino acid solution at room temperature. The mixed solution was shaken for a few seconds to obtain a homogeneous dispersion. The samples were allowed to stand at room temperature for different times (3, 10, 16 h, and 5 days for Fmoc-P, Fmoc-H, Fmoc-A, and Fmoc-L metallohydrogels, respectively) to obtain stable hydrogels.

Morphological Characterization of Metallohydrogels: The surface microstructures of the materials were analyzed by AFM and TEM. For these measurements, the metallohydrogels prepared with amino acid and Ag^+ concentrations of 4 mg mL^{-1} and 8 × 10^{-3} M were smeared on a silicon wafer or copper grid and blotted with a filter paper to obtain a thin liquid film, followed by the vacuum drying. AFM images were collected using a FASTSCANBIO (Bruker) in a tapping mode and TEM measurement was carried out on a JEM-1011 microscope (JEOL, Japan).

Spectral Characterization of Metallohydrogels: Circular dichroism spectra were recorded at room temperature using a JASCO J-815 spectrometer (quartz cell, path length = 1 mm). Each spectrum is the average of three measurements. FTIR spectra were measured on a TENSOR 27 FTIR spectrometer (Bruker) using KBr pressed disks. The XRD patterns of the freeze-dried Fmoc-amino acid metallohydrogels were collected on a Rigaku D/max-2500 instrument under the following conditions: scanned from 2° to 40° (2θ value) at a scanning speed of 5° min^{-1}. Freeze-dried metallohydrogels were obtained as follows. Fmoc-amino acid hydrogels were prepared in centrifuge tubes and placed into a lab freezer at –80 °C for ≈2 h before being placed into a vacuum freeze-dryer with a condenser temperature of –40 °C and a shelf temperature of –20 °C for 12 h.

Rheological Test: Rheology experiments were performed on an Anton Paar MCR 302 rheometer at 25 °C. The hydrogel samples were prepared in a glass vessel with a constant inner diameter of 15 mm and height of 0.5 mm and then gently transferred using a spatula to the middle of a 15 mm diameter parallel plate with a constant gap of 0.5 mm. Strain-dependent oscillatory rheology sweep was performed in the range of 0.1–100% at a constant frequency of 10 rad s^{-1}. Dynamic oscillatory frequency sweep ranging from 0.1 to 100 Hz was conducted at a 1% strain amplitude. Strain-induced damage and self-healing property of the hydrogels were tested with the oscillatory strain between 500% and 1% and frequency of 1 rad s^{-1}. To prevent the evaporation of water, a lid was placed on the top of the sample.

Density Functional Theory Calculations: To determine the coordination environment of Ag^+ within the $[Fmoc\text{-}AA\cdots Ag]^+$ complex, density functional theory calculations were carried out using the Gaussian09 package. Full geometry optimizations of the $[Fmoc\text{-}AA\cdots Ag]^+$ complex with different structures in the gas phase were carried out using the Becke three-parameter hybrid (B3LYP) exchange-correlation functional without symmetry constrains. The standard split-valence 6–311G (d,p) basis set of atomic orbitals was used for H, C, N, O atoms and the Ag^+ was described by the LANL2DZ relativistic pseudopotentials. The harmonic vibrational frequency calculations on the optimized geometries were also performed to ensure the structures at local minima.

Bacteria Culture: Gram-positive bacteria of *S. aureus* (ATCC 6538), Gram-negative bacteria of *E. coli* (ATCC 8739) were used in the experiments. *S. aureus* and *E. coli* were grown at 37 °C and maintained in a Langmuir–Blodgett (LB) liquid medium (1% tryptone, 0.5% yeast

extract, 1% NaCl, pH = 7) or LB solid medium (1% tryptone, 0.5% yeast extract, 1% NaCl, and 1.5% Agar pH = 7).

Inhibition Zone Test: Oxford cup methods were used to examine the antibacterial activity against two bacterial strains: *E. coli*, *S. aureus*. In antibacterial tests, 1 mL freshly grown bacteria was added into 30 mL warm LB agar broth to form an LB-bacterial mixed solution. 15 mL pure LB agar broth poured into 100 mm aseptic Petri dishes. 5 mL LB-bacterial mixed solution was then injected into Petri dishes when the pure medium solidification. Four Oxford cups were planted in the surface of above medium. 200 µL supramolecular metallohydrogels, amino acid solution, Ag^+ solution, and PBS buffer were injected into the four Oxford Cups. The plates were incubated at 37 °C overnight. Colonies were visualized and digital images were captured on the next day.

Reduction of Cell Growth: Reduction of cell growth of Fmoc-amino acid metallohydrogels was measured using a broth microdilution method. First, the bacterial solution was diluted with LB broth to get suspension with 0.1 OD, which incubated at 37 °C for 2 h to get bacterial mid-log phase. The diluted bacterial solution was then equally distributed into Erlenmeyer flasks. Fmoc-amino acid metallohydrogels were added into the above bacterial solution (final concentration of 1×10^{-3} M on the basis of Ag). Ag^+ solution (final concentration of 1×10^{-3} M) and ultrapure water were added as control, respectively. The bacterial were then grown at 37 °C, 200 rpm for 1 week. Samples were withdrawn from the bacterial solution every 12 h, and the bacterial growth was measured at 600 nm with microplate reader. The experiments were repeated three times.

Minimum Inhibitory Concentration Test: Different concentrations of the Fmoc-amino acid metallohydrogels were obtained by dilution 10-time, 20-time, 80-time, and 160-time of the initial gels (prepared with 8×10^{-3} M Ag^+ and 4 mg mL^{-1}) and 8×10^{-3} M Ag^+ solution in bacterial solution as the experimental group. Fmoc-amino acids (final concentration of 0.4 mg mL^{-1}) and ultrapure water were added into bacterial solution as control, respectively. The optical density readings of microorganism solutions were measured after 24 and 48 h of incubation. All the tests were repeated three times.

3-(4,5-Dimethylthiazolyl-2)-2,5-diphenyltetrazolium Bromide (MTT) Experiment: A mouse embryonic fibroblast cell line NIH-3T3 was chosen for the MTT experiment. Cells were cultured in DMEM containing 10% bovine serum, 1% penicillin, and 1% streptomycin at 37 °C at a 5% CO_2 environment. The hydrogels (prepared with 8×10^{-3} M Ag^+ and 4 mg mL^{-1} Fmoc-amino acid) were broken by high shear force and diluted in cell medium (final concentration of 50 and 12.5×10^{-6} M on the basis of Ag) as experimental group. Fmoc-amino acids stock solution were added into cell medium, with a final concentration of 0.4 mg mL^{-1} and blank cell medium as control group. Both the experimental and control groups were coincubated with the cells for 24 h. The cells were washed thrice with PBS to remove the dead cells, followed by the addition of MTT (10 µL, 5 mg mL^{-1} thiazole blue) into each well. After 4 h, the medium was replaced by 100 µL DMSO. The absorbance of dissolved medium was measured using a microplate reader at 570 nm.

Morphology Study of Bacteria: First, Fmoc-amino acid metallohydrogels were added into the bacterial solution (final concentration of 1×10^{-3} M on the basis of Ag). Ag^+ solution (final concentration of 1×10^{-3} M) and ultrapure water were added as control, respectively. After 12 h, the bacterial were collected by centrifugation and then fixed with 2% glutaraldehyde for 15 min, washed with distilled water to eliminate the remaining glutaraldehyde. Next, the fixed bacteria were dropped onto copper mesh or wafer and then freeze-dried to maintain the morphologies of the bacteria captured on substrate. After complete drying, the bacteria on the copper mesh were imaged with TEM microscope (JEOL-1011, JEOL, Japan) and SEM microscopy (S-4800, HITACHI, Japan).

Animal Experiments: Adult female BALB/c mice (ages, 6 to 8 weeks; weights, 17 to 21 g; Vital Laboratory Animal Center (Beijing, China)) were used in the study. The animals were housed at one mouse per cage and were maintained on a 12 h light–12 h dark cycle with access to food and water ad libitum. Next, a 1 cm length wound was cut with scissors on the back of each mouse down to the panniculus carnosus, which was generated in the center of the lower back after shaving and cleansing with alcohol. There was no visible bleeding within the wounds. The mice were euthanized according to the protocol when their condition was assessed to be moribund. All animal experiments were performed in compliance with the Guide for the Care and Use of Laboratory Animals, and were approved by the Experimental Animal Ethics Committee in Beijing.

In Vivo Infection Study: Thirty minutes after anesthetized mice received single wounds measuring 1 cm, they received inocula of mid-log phase *S. aureus* = $25*10^7$ cells bacteria suspended in 10 µL PBS or just 10 µL PBS and applied with a 10 µL pipette tip into the wound bed. Mice were imaged in camera immediately after infection and then daily until sacrifice. Shear-thinning Fmoc-amino acid metallohydrogels (100 µL, prepared with 4 mg mL^{-1} Fmoc-amino acids and 8×10^{-3} M Ag^+) or antimicrobial cream (with equivalent amount of Ag^+) were applied to the infected wounds for 30 min. Six experimental groups consisting of (1) Fmoc-H metallohydrogel, (2) Fmoc-P metallohydrogel, (3) Fmoc-A metallohydrogel, (4) Fmoc-L metallohydrogel, (5) control group without treatment, and (6) SSD cream were used for the affection of *S. aureus* and no affection just wound animal experiments.

Supporting Information

Supporting Information is available from the Wiley Online Library or from the author.

Acknowledgements

J.S. and C.Y. contributed equally to this work. All animal experiments were performed in compliance with the Guide for the Care and Use of Laboratory Animals, and were approved by the Experimental Animal Ethics Committee in Beijing. This work was financially supported by the National Natural Science Foundation of China (Project Nos. 21773248, 21802143, and 21802144), the National Natural Science Fund BRICS STI Framework Programme (No. 51861145304), the Key Research Program of Frontier Sciences of Chinese Academy of Sciences (CAS, Grant No. QYZDB-SSW-JSC034), and the CAS President's International Fellowship Initiative (2018VEA0005) as well as the EPSRC for a Fellowship (EP/L021978/1).

Conflict of Interest

The authors declare no conflict of interest.

Keywords

amino acids, antimicrobial, biometallohydrogels, broad-spectrum, coordinated self-assembly

Received: December 15, 2019
Revised: December 30, 2019
Published online: January 29, 2020

[1] a) G. Taubes, *Science* **2008**, *321*, 356; b) M. A. Fischbach, C. T. Walsh, *Science* **2009**, *325*, 1089; c) L. Ejim, M. A. Farha, S. B. Falconer, J. Wildenhain, B. K. Coombes, M. Tyers, E. D. Brown, G. D. Wright, *Nat. Chem. Biol.* **2011**, *7*, 348; d) X. Li, H. Bai, Y. Yang, J. Yoon, S. Wang, X. Zhang, *Adv. Mater.* **2019**, *31*, 1805092.

[2] a) D. J. Phillips, J. Harrison, S.-J. Richards, D. E. Mitchell, E. Tichauer, A. T. M. Hubbard, C. Guy, I. Hands-Portman,

E. Fullam, M. I. Gibson, *Biomacromolecules* **2017**, *18*, 1592; b) Y. Yang, Z. Cai, Z. Huang, X. Tang, X. Zhang, *Polym. J.* **2018**, *50*, 33; c) E. F. Palermo, K. Lienkamp, E. R. Gillies, P. J. Ragogna, *Angew. Chem., Int. Ed.* **2019**, *58*, 3690.

[3] a) L. Liu, K. Xu, H. Wang, P. K. Jeremy Tan, W. Fan, S. S. Venkatraman, L. Li, Y.-Y. Yang, *Nat. Nanotechnol.* **2009**, *4*, 457; b) J. Hu, C. Chen, S. Zhang, X. Zhao, H. Xu, X. Zhao, J. R. Lu, *Biomacromolecules* **2011**, *12*, 3839; c) L. Schnaider, S. Brahmachari, N. W. Schmidt, B. Mensa, S. Shaham-Niv, D. Bychenko, L. Adler-Abramovich, L. J. W. Shimon, S. Kolusheva, W. F. DeGrado, E. Gazit, *Nat. Commun.* **2017**, *8*, 1365; d) Z. Yang, G. Liang, Z. Guo, Z. Guo, B. Xu, *Angew. Chem., Int. Ed.* **2007**, *46*, 8216; e) M. Cao, W. Zhao, L. Wang, R. Li, H. Gong, Y. Zhang, H. Xu, J. Lu, *ACS Appl. Mater. Interfaces* **2018**, *10*, 24937; f) K. Ariga, T. Makita, M. Ito, T. Mori, S. Watanabe, J. Takeys, *Beilstein J. Nanotechnol.* **2019**, *10*, 2014.

[4] a) J. A. Lemire, J. J. Harrison, R. J. Turner, *Nat. Rev. Microbiol.* **2013**, *11*, 371; b) L. Rizzello, P. P. Pompa, *Chem. Soc. Rev.* **2014**, *43*, 1501; c) K. Ariga, J. B. Li, J. B. Fei, Q. M. Ji, J. P. Hill, *Adv. Mater.* **2016**, *28*, 1251.

[5] a) X. Ding, S. Duan, X. Ding, R. Liu, F. Xu, *Adv. Funct. Mater.* **2018**, *28*, 1802140; b) A. G. Cheetham, R. W. Chakroun, W. Ma, H. G. Cui, *Chem. Soc. Rev.* **2017**, *46*, 6638.

[6] R. Eckert, *Future Microbiol.* **2011**, *6*, 635.

[7] a) J. B. Wright, K. Lam, A. G. Buret, M. E. Olson, R. E. Burrell, *Wound Repair Regener.* **2002**, *10*, 141; b) V. Alt, T. Bechert, P. Steinrücke, M. Wagener, P. Seidel, E. Dingeldein, E. Domann, R. Schnettler, *Biomaterials* **2004**, *25*, 4383; c) D. J. Leaper, *Int. Wound J.* **2006**, *3*, 282.

[8] P. Yuan, X. Ding, Y. Y. Yang, Q.-H. Xu, *Adv. Healthcare Mater.* **2018**, *7*, 1701392.

[9] a) I. Irwansyah, Y.-Q. Li, W. Shi, D. Qi, W. R. Leow, M. B. Y. Tang, S. Li, X. Chen, *Adv. Mater.* **2015**, *27*, 648; b) S. Li, S. Dong, W. Xu, S. Tu, L. Yan, C. Zhao, J. Ding, X. Chen, *Adv. Sci.* **2018**, *5*, 1700527.

[10] a) R. Xing, K. Liu, T. Jiao, N. Zhang, K. Ma, R. Zhang, Q. Zou, G. Ma, X. Yan, *Adv. Mater.* **2016**, *28*, 3669; b) R. Xing, S. Li, N. Zhang, G. Shen, H. Möhwald, X. Yan, *Biomacromolecules* **2017**, *18*, 3514; c) X. Jia, K. Minami, K. Uto, A. Chang, J. Hill, J. Nakanishi, K. Ariga, *Adv. Mater.* **2020**, *32*, 1905942.

[11] a) G. Meng, A. Grabiec, M. Vallon, B. Ebe, S. Hampel, W. Bessler, H. Wagner, C. J. Kirschning, *J. Biol. Chem.* **2003**, *278*, 39822; b) R. M. Burch, M. Weitzberg, N. Blok, R. Muhlhauser, D. Martin, S. G. Farmer, J. M. Bator, J. R. Connor, M. Green, C. Ko, *Proc. Natl. Acad. Sci. USA* **1991**, *88*, 355; c) K. Liu, R. Xing, Y. Li, Q. Zou, H. Möhwald, X. Yan, *Angew. Chem., Int. Ed.* **2016**, *55*, 12503.

[12] a) J. Wang, K. Liu, R. Xing, X. Yan, *Chem. Soc. Rev.* **2016**, *45*, 5589; b) Y. Li, Q. Zou, C. Yuan, S. Li, R. Xing, X. Yan, *Angew. Chem., Int. Ed.* **2018**, *57*, 17084; c) X. Ren, Q. Zou, C. Yuan, R. Chang, R. Xing, X. Yan, *Angew. Chem., Int. Ed.* **2019**, *58*, 5872; d) J. Zhan, Y. Cai, S. He, L. Wang, Z. Yang, *Angew. Chem., Int. Ed.* **2018**, *57*, 1813; e) C. Yuan, W. Ji, R. Xing, J. Li, E. Gazit, X. Yan, *Nat. Rev. Chem.* **2019**, *3*, 567.

[13] S. J. Lam, N. M. O'Brien-Simpson, N. Pantarat, A. Sulistio, E. H. H. Wong, Y.-Y. Chen, J. C. Lenzo, J. A. Holden, A. Blencowe, E. C. Reynolds, G. G. Qiao, *Nat. Microbiol.* **2016**, *1*, 16162.

[14] a) S. Basak, J. Nanda, A. Banerjee, *Chem. Commun.* **2014**, *50*, 2356; b) K. Tao, A. Levin, L. Adler-Abramovich, E. Gazit, *Chem. Soc. Rev.* **2016**, *45*, 3935; c) S. Fleming, R. V. Ulijn, *Chem. Soc. Rev.* **2014**, *43*, 8150.

[15] Z. Fan, B. Liu, J. Wang, S. Zhang, Q. Lin, P. Gong, L. Ma, S. Yang, *Adv. Funct. Mater.* **2014**, *24*, 3933.

[16] a) E. Pazos, E. Sleep, C. M. Rubert Pérez, S. S. Lee, F. Tantakitti, S. I. Stupp, *J. Am. Chem. Soc.* **2016**, *138*, 5507; b) Y. Wang, L. Cao, S. Guan, G. Shi, Q. Luo, L. Miao, I. Thistlethwaite, Z. Huang, J. Xu, J. Liu, *J. Mater. Chem.* **2012**, *22*, 2575; c) L. Yu, I. A. Banerjee, H. Matsui, *J. Am. Chem. Soc.* **2003**, *125*, 14837.

[17] C. Yuan, A. Levin, W. Chen, R. Xing, Q. Zou, T. W. Herling, P. K. Challa, T. P. J. Knowles, X. Yan, *Angew. Chem., Int. Ed.* **2019**, *58*, 18116.

[18] D. S. Su, T. Jacob, T. W. Hansen, D. Wang, R. Schlögl, B. Freitag, S. Kujawa, *Angew. Chem., Int. Ed.* **2008**, *47*, 5005.

[19] S. Corra, M. S. Shoshan, H. Wennemers, *Curr. Opin. Chem. Biol.* **2017**, *40*, 138.

[20] N. C. Polfer, J. Oomens, D. T. Moore, G. von Helden, G. Meijer, R. C. Dunbar, *J. Am. Chem. Soc.* **2006**, *128*, 517.

[21] a) R. Xing, C. Yuan, S. Li, J. Song, J. Li, X. Yan, *Angew. Chem., Int. Ed.* **2018**, *57*, 1537; b) S. Bera, S. Mondal, S. Rencus-Lazar, E. Gazit, *Acc. Chem. Res.* **2018**, *51*, 2187.

[22] a) A. M. Smith, R. J. Williams, C. Tang, P. Coppo, R. F. Collins, M. L. Turner, A. Saiani, R. V. Ulijn, *Adv. Mater.* **2008**, *20*, 37; b) Z. Yang, L. Wang, J. Wang, P. Gao, B. Xu, *J. Mater. Chem.* **2010**, *20*, 2128.

[23] a) V. J. Bradford, B. L. Iverson, *J. Am. Chem. Soc.* **2008**, *130*, 1517; b) C. Yan, D. Pochan, *Chem. Soc. Rev.* **2010**, *39*, 3528.

[24] a) C. Yan, D. J. Pochan, *Chem. Soc. Rev.* **2010**, *39*, 3528; b) C. B. Highley, C. B. Rodell, J. A. Burdick, *Adv. Mater.* **2015**, *27*, 5075; c) L. Li, B. Yan, J. Yang, L. Chen, H. Zeng, *Adv. Mater.* **2015**, *27*, 1294.

[25] A. K. Marr, W. J. Gooderham, R. E. W. Hancock, *Curr. Opin. Pharmacol.* **2006**, *6*, 468.

[26] X. Yuan, M. I. Setyawati, D. T. Leong, J. Xie, *Nano Res.* **2014**, *7*, 301.

[27] O. Brandt, M. Mildner, A. E. Egger, M. Groessl, U. Rix, M. Posch, B. K. Keppler, C. Strupp, B. Mueller, G. Stingl, *Nanomed. Nanotechnol. Biol. Med.* **2012**, *8*, 478.

[28] a) Q. L. Feng, J. Wu, G. Q. Chen, F. Z. Cui, T. N. Kim, J. O. Kim, *J. Biomed. Mater. Res.* **2000**, *52*, 662; b) W. K. Jung, H. C. Koo, K. W. Kim, S. Shin, S. H. Kim, Y. H. Park, *Appl. Environ. Microbiol.* **2008**, *74*, 2171.

[29] P.-H. Chan, Y.-C. Chen, *Anal. Chem.* **2012**, *84*, 8952.

[30] M. L. Mangoni, A. M. McDermott, M. Zasloff, *Exp. Dermatol.* **2016**, *25*, 167.

[31] X. Zhao, H. Wu, B. Guo, R. Dong, Y. Qiu, P. X. Ma, *Biomaterials* **2017**, *122*, 34.

[32] a) Q. Zou, X. Yan, *Chem. - Eur. J.* **2018**, *24*, 755; b) S. Li, Q. Zou, Y. Li, C. Yuan, R. Xing, X. Yan, *J. Am. Chem. Soc.* **2018**, *140*, 10794; c) H. Sun, R. Chang, Q. Zou, R. Xing, W. Qi, X. Yan, *Small* **2019**, *15*, 1905326.